Inorg. Chem. **2004**, *43*, 1933–1942

Reactions of *arachno*-6,8-$C_2B_7H_{12}^-$ with Electron Deficient Olefins: Syntheses of Cyano-Substituted Carboranes

Daniel E. Kadlecek, Daewon Hong, Patrick J. Carroll, and Larry G. Sneddon*

Department of Chemistry, University of Pennsylvania, Philadelphia, Pennsylvania 19104-6323

Received November 24, 2003

The syntheses of new cyano-substituted derivatives of *arachno*-6,8-$C_2B_7H_{13}$ have been achieved through the addition reactions of the *arachno*-6,8-$C_2B_7H_{12}^-$ (**1**$^-$) anion with cyano-activated olefins. The reaction of **PSH**$^+$**1**$^-$ with tetracyanoethylene (TCNE) yielded the unusual bridging compound PSH$^+$*endo*-6-*endo*-7-[μ_2-$(C(CN)_2)_2$]-*arachno*-6,8-$C_2B_7H_{12}^-$ (**PSH**$^+$**2**$^-$) resulting from cycloaddition of the TCNE at the C6–B7 edge of the anion. Consistent with its *hypho* skeletal electron count, an X-ray crystallographic study and DFT/GIAO calculations confirm **2**$^-$ has a more open structure than **1**$^-$. The reaction of **1**$^-$ with acrylonitrile resulted in the formation of *endo*-6-$(NCCH_2CH_2)$-*arachno*-6,8-$C_2B_7H_{11}^-$ (**3**$^-$), which, upon acidification, afforded *endo*-6-$(NCCH_2CH_2)$-*arachno*-6,8-$C_2B_7H_{12}$ (**3**) in high yield. X-ray crystallographic and DFT/GIAO studies established that the cyanoethyl fragment in **3** is substituted at the *endo*-position of the C6 cage-carbon. Heating **3** in THF at 50 °C or in toluene at 110 °C resulted in the quantitative isomerization of the cyanoethyl-substituent from the *endo*- to the *exo*-position at C6 to yield *exo*-6-$(NCCH_2CH_2)$-*arachno*-6,8-$C_2B_7H_{12}$ (**4**). This is the first example of an *endo* to *exo* isomerization to be observed at a cage-carbon of a carborane. While heating **3** resulted in isomerization to **4**, heating **3**$^-$ in the presence of a small amount of **3** yielded the new ethylene-bridged 10-vertex tricarbaborane $\mu_{6,9}$-(CH_2CH_2)-*arachno*-5,6,9-$C_3B_7H_{11}$ (**5**) resulting from reduction of the **3**$^-$ pendant nitrile group, followed by deammination and carbon insertion.

Introduction

We have previously shown that the *arachno*-6,8-$C_2B_7H_{12}^-$ (**1**$^-$) anion is a good nucleophile that will readily add to multiple bonds in nitriles or polarized alkynes containing electron-withdrawing substituents. We have also shown that such reactions can ultimately provide high yield pathways to polyborane carbon-insertion products.[1] In this paper, we report that **1**$^-$ will likewise add to the electron-deficient cyano-substituted olefins tetracyanoethylene and acrylonitrile to yield new types of cyano-carboranes. Furthermore, we report both the discovery of a new type of *endo* to *exo* isomerization reaction and the formation of a basketlike tricarbaborane resulting from the reaction of a pendant nitrile substituent of a cyano-substituted dicarbaborane.

Experimental Section

All manipulations were carried out using standard high-vacuum or inert-atmosphere techniques as described by Shriver.[2]

Materials. Acrylonitrile, tetracyanoethylene, 1,8-bis(dimethylamino)naphthalene (proton sponge, PS), and $HCl-OEt_2$ were purchased from Aldrich and used as received. Oil dispersed NaH was purchased from Aldrich, washed with dry hexanes under a N_2 atmosphere, and dried under high-vacuum prior to use. The 1,2-dimethoxyethane (DME), toluene, acetonitrile, and dichloromethane were dried by passing through an activated alumina column prior to use. THF was purified by distillation from sodium/benzophenone ketyl. Pentane was used as received. The *arachno*-6,8-$C_2B_7H_{13}$ was prepared according to literature procedures.[3]

Physical Measurements. ^{1}H NMR spectra at 500.4 MHz, ^{11}B NMR spectra at 160.5 MHz, and ^{13}C NMR at 125.8 MHz were obtained on a Bruker AM-500 spectrometer equipped with the appropriate decoupling accessories. ^{11}B NMR spectra at 64.2 MHz were obtained on a Bruker AF-200 spectrometer. NMR data are presented in Table 1. All ^{11}B chemical shifts are referenced to external BF_3-OEt_2 (0.00 ppm) with a negative sign indicating an upfield shift. All ^{1}H and ^{13}C chemical shifts were measured relative to internal residual protons or carbons in the lock solvent and are referenced to Me_4Si (0.00 ppm). High-resolution mass spectra (HRMS) were recorded on a Micromass Autospec spectrometer.

(1) (a) Kang, S. O.; Furst, G. T.; Sneddon, L. G. *Inorg. Chem.* **1989**, *28*, 2339−2347. (b) Plumb, C. A.; Carroll, P. J.; Sneddon, L.G. *Organometallics* **1992**, *11*, 1665−1671. (c) Su, K.; Carroll, P. J.; Sneddon, L. G. *J. Am. Chem. Soc.* **1993**, *115*, 10004−10017. (d) Wille, A. E.; Sneddon, L. G. *Collect. Czech. Chem. Commun.* **1997**, *62*, 1214−1228.

(2) Shriver, D. F.; Drezdzon, M. A. *Manipulation of Air-Sensitive Compounds*, 2nd ed.; Wiley: New York, 1986.

(3) Garrett, P. M.; George, T. A.; Hawthorne, M. F. *Inorg. Chem.* **1969**, *8*, 2008−9.

10.1021/ic035357t CCC: $27.50
Published on Web 02/17/2004

Table 1. NMR Data

compds	nucleus	δ (multiplicity, intensity, assignment, J (Hz))
Na^+1^-	$^{11}B^{a,b}$	10.8 (d, B5, J_{BH} 139), −1.8 (d, B7, J_{BH} 139), −16.4 (d, B3, J_{BH} 150), −19.9 (d, B9, J_{BH} 174), −37.3 (d, B1, J_{BH} 135), −43.7 (m, B4), −48.0 (d, B2, J_{BH} 146)
I^-	^{11}B(calcd)^c	15.4 (B5), −2.7 (B7), −15.8 (B3), −27.1 (B9), −36.9 (B1), −44.9 (B4), −51.4 (B2)
PSH^+2^-	$^{11}B^{d,e}$	5.1 (d, B9, J_{BH} 149), −1.2 (d, B7, J_{BH} 132), −4.9 (d, B5, J_{BH} 96), −12.7 (d, B3, J_{BH} 149), −20.3 (d, B4, J_{BH} 149), −25.0 (d, B2, J_{BH} 130), −55.6 (d, B1, J_{BH} 143)
	$^1H\{^{11}B\}^{f,e}$	19.26 (s, 1, PS*H*$^+$), 7.76−8.08 (m, 6, Ph, PSH^+), 3.73 (1, BH), 3.20 (s, 12, Me, PSH^+), 3.08 (1, BH), 2.52 (1, BH), 2.40 (1, BH), 1.82 (2, BH, cage-CH^h), 1.13 (1, BH), 0.29 (s, 1, cage-CH), −0.78 (1, BH), −0.91 (s, 1, cage-CH), −2.13 (1, BHB), −2.66 (1, BHB)
	$^{13}C\{^1H\}^{g,e}$	15.9 (C6), −17.6 (C8)
II^-	^{11}B(calcd)^c	2.3 (B9), 0.5 (B7), −7.3 (B5), −12.4 (B3), −22.8 (B4), −24.9 (B2), −59.3 (B1)
	^{13}C(calcd)^c	23.9 (C6), −15.7 (C8)
Na^+3^-	$^{11}B^{a,d}$	9.5 (d, B9, J_{BH} 135), 0.0 (d, B2, J_{BH} 137), −4.3 (d, B7, J_{BH} 143), −18.7 (d, B5, J_{BH} 104), −34.9 (d, B1, J_{BH} 133), −42.1 (m, B4)^h, −45.7 (d, B3, J_{BH} 147)
	$^1H\{^{11}B\}^{a,f}$	3.01 (m, 2, CH_2CH_2CN), 2.85 (m, 2, CH_2CH_2CN), 2.43 (1, BH), 2.18 (s, 1, cage-CH), 2.03 (1, BH), 1.50 (1, BH), 0.97 (s, 1, cage-CH), 0.35 (s, 1, cage-CH), −0.08 (2, BH), −0.46 (1, BH), −0.58 (1, BH), −1.12 (1, BH), −5.17 (BHB)
	$^{13}C\{^1H\}^{a,g}$	121.4 (CH_2CH_2CN), 62.6 (C8), 41.5 (CH_2CH_2CN), 20.6 (CH_2CH_2CN), 1.8 (C6)
IIIa$^-$	^{11}B(calcd)^c	16.6 (B9), 1.2 (B2), −3.5 (B7), −21.4 (B5), −34.0 (B1), −40.9 (B4), −46.5 (B3)
	^{13}C(calcd)^c	125.3 (CH_2CH_2CN), 77.6 (C8), 48.2 (CH_2CH_2CN), 22.8 (CH_2CH_2CN), 9.4 (C6)
3	$^{11}B^{d,i}$	5.4 (d, B9, J_{BH} 174), 4.2 (d, B5, J_{BH} 168), 0.3 (d, B2, J_{BH} 161), −0.7 (d, B7, J_{BH} 157), −13.5 (d, B3, J_{BH} 163), −21.3 (d, B4, J_{BH} 143), −49.0 (d, B1, J_{BH} 153)
	^{11}B-$^{11}B^{d,e}$	Observed cross-peaks: B1−B2; B1−B3; B1−B4; B1−B5; B1−B9; B2−B3; B2−B5; B3−B7; B3−B9; B4−B5; B4−B9
	$^1H\{^{11}B\}^{f,e}$	3.41 (1, BH), 3.32 (1, BH), 3.23 (2, BH), 2.59 (m, 2, CH_2CH_2CN), 2.39 (1, BH), 2.34 (m, 1, CH_2CH_2CN), 2.27 (1, BH), 1.05 (m, 1, CH_2CH_2CN), 0.54 (s, 1, cage-CH), 0.47 (s, 1, cage-CH), −0.12 (1, BH), −0.44 (m, 1, cage-CH), −1.45 (1, BHB), −2.92 (1, BHB)
	$^{13}C\{^1H\}^{g,h}$	118.2 (CH_2CH_2CN), 46.2 (CH_2CH_2CN), 22.5 (CH_2CH_2CN), 4.8 (C6), −9.6 (C8)
IIIa	^{11}B(calcd)^c	4.7 (B9), 4.5 (B5), 2.6 (B2), −2.7 (B7), −9.4 (B3), −21.6 (B4), −52.1 (B1)
	^{13}C(calcd)^c	119.9 (CH_2CH_2CN), 52.3 (CH_2CH_2CN), 24.0 (CH_2CH_2CN), 10.7 (C6), −8.4 (C8)
IIIb	^{11}B(calcd)^c	4.6 (B9), 2.9 (B2), 2.5 (B7), 1.7 (B5), −12.4 (B3), −23.1 (B4), −50.4 (B1)
	^{13}C(calcd)^c	119.8 (CH_2CH_2CN), 52.1 (CH_2CH_2CN), 23.3 (CH_2CH_2CN), 8.1 (C6), −8.3 (C8)
4	$^{11}B^{d,e}$	3.1 (d, B5, J_{BH} 113), 2.4 (d, B7, J_{BH} 162), 0.4 (d, B9, J_{BH} 149), −14.5 (d, B2, J_{BH} 155), −17.4 (d, B3, J_{BH} 162), −27.5 (d, B4, J_{BH} 156), −52.0 (d, B1, J_{BH} 154)
	^{11}B-$^{11}B^{d,e}$	obsd cross-peaks: B1−B2; B1−B3; B1−B4; B1−B5; B1−B9; B2−B3; B2−B5; B2−B7; B3−B7; B3−B9
	$^1H\{^{11}B\}^{f,e}$	3.36 (1, BH), 3.24 (1, BH), 3.18 (1, BH), 2.52 (t, 2, CH_2CH_2CN), 2.16 (2, BH), 1.97 (3, BH, $CH_2CH_2CN^h$), 0.33 (s, 1, cage-CH), −0.21 (1, BH), −0.49 (s, 1, cage-CH), −0.58 (s, 1, cage-CH), −1.81 (1, BHB), −2.11 (1, BHB)
	$^{13}C\{^1H\}^{g,e}$	119.7 (CH_2CH_2CN), 29.7 (CH_2CH_2CN), 18.8 (CH_2CH_2CN), 2.9 (C6), −11.8 (C8)
IV	^{11}B(calcd)^c	6.9 (B5), 0.1 (B9), −1.8 (B7), −12.1 (B2), −13.1 (B3), −27.8 (B4), −55.3 (B1)
	^{13}C(calcd)^c	120.3 (CH_2CH_2CN), 36.4 (CH_2CH_2CN), 21.1 (CH_2CH_2CN), 10.7 (C6), −9.6 (C8)
PSH^+4^-	$^{11}B^{b,j}$	9.3 (d, B9, J_{BH} 122), −2.7 (d, B7, J_{BH} 135), −17.2 (d, B2, J_{BH} 164), −20.9 (d, B5, J_{BH} 138), −38.4 (d, B1, J_{BH} 136), −44.5 (m, B4)^h, −46.8 (d, B3, J_{BH} 149)
IV$^-$	^{11}B(calcd)^c	16.0 (B9), 2.0 (B7), −15.1 (B2), −25.7 (B5), −36.9 (B1), −46.3 (B4), −49.7 (B3)
5	$^{11}B^{d,e}$	9.4 (d, J_{BH} 174), 4.6 (d, J_{BH} 160), −8.4 (d, J_{BH} 150)^h, −9.5 (d, J_{BH} 160)^h, −14.2 (d, J_{BH} 145, $J_{BH(br)}$ 37), −27.4 (d, J_{BH} 158), −40.9 (d, J_{BH} 149)
	$^1H\{^{11}B\}^{f,e}$	3.50 (BH), 3.08 (BH), 2.52 (BH), 2.47 (BH), 2.43 (BH), 2.31 (BH), 2.23 (CH_2), 2.12 (BH), 1.37 (CH_2), 0.40 (CH), ∼0.3 (CH), −0.03 (CH), −2.71 (BHB)
	$^{13}C\{^1H\}^{g,e}$	35.9 (qr, J_{CB} 35), 30.0 (CH_2), 23.9 (CH_2), 18.6 (C6), 11.2 (C9)
V	^{11}B(calcd)^c	12.0 (B2), 6.8 (B4), −7.5 (B10), −10.2 (B8), −16.8 (B7), −28.7 (B1), −40.5 (B3)
	^{13}C(calcd)^c	43.9 (C5), 34.7 (C11), 29.0 (C12), 23.0 (C6), 17.7 (C9)

[a] CD_3CN. [b] 64.2 MHz. [c] B3LYP/6-311G*//B3LYP/6-311G*. [d] 160.5 MHz. [e] CD_2Cl_2 [f] 500.4 MHz. [g] 125.8 MHz. [h] Overlapped. [i] THF-d_8. [j] THF.

FT-IR and diffuse-reflectance IR (DRIFT) spectra were obtained on a Perkin-Elmer System 2000 FT-IR. Melting points were obtained on a standard melting point apparatus and are uncorrected.

PSH^+*endo*-6-*endo*-7-[μ_2-$(C(CN)_2)_2$]-*arachno*-6,8-$C_2B_7H_{12}^-$ (PSH^+2^-). A 100-mL, two-neck, round-bottom flask fitted with a vacuum adapter, stirbar, and septum was charged with 0.34 g (3.0 mmol) of *arachno*-6,8-$C_2B_7H_{13}$ and 0.42 g (3.3 mmol) of tetracyanoethylene under a N_2 flow. DME (10 mL) was added with stirring to dissolve the reactants, and the solution then cooled at 0 °C. A solution of 0.71 g (3.3 mmol) of proton sponge dissolved in 5 mL of DME was then added dropwise via syringe to the reaction flask turning the solution a dark brown. The solution was then left to stir for 12 h with slow warming to room temperature. After ^{11}B NMR analysis indicated the reaction was complete, the solution was filtered in the glovebag and the reaction solid washed 3 times with 10 mL portions of DME. The filtrate and washings were combined and the volatiles removed under reduced pressure to yield an orange-brown oil which was then dried overnight on the high-vacuum line. The oil was next dissolved in 5 mL of CH_2Cl_2, and then, 10 mL of hexanes was added dropwise to precipitate the oil, leaving a slightly cloudy, yellow supernatant. The supernatant was collected, and the procedure was repeated 10 times at which point the solutions were combined and concentrated under reduced pressure to afford 0.54 g (1.2 mmol, 40%) of a yellow, powdery solid identified as PSH^+*endo*-6-*endo*-7-[μ_2-$(C(CN)_2)_2$]-*arachno*-6,8-$C_2B_7H_{12}^-$ (**PSH^+2^-**). Anal. Calcd: C, 58.05; H, 6.86; N, 18.46. Found: C, 57.07; H, 6.99; N, 18.88. HRMS (ESI−) (*m*/*e*) calcd for $^{12}C_8{}^{11}B_7{}^{14}N_4{}^1H_{12}$ (anion fragment) 241.1713, found 241.1717; IR (DRIFT, KBr, cm^{-1}) 3055 (w), 2983 (w), 2567 (s), 2528 (vs), 2485 (s), 2248 (m), 1956 (w), 1831 (w), 1604 (w), 1559 (w), 1541 (w), 1464 (s), 1411 (w), 1271 (w), 1221 (w), 1161 (w), 1036 (w), 955 (m), 834 (m), 771 (s), 690 (w), 633 (w), 596 (w).

Acidification of **PSH^+2^-** was attempted by two methods. First, 0.20 g (0.44 mmol) of **PSH^+2^-** dissolved in 5 mL of DME was

maintained at 0 °C while 0.5 mL of HCl−OEt_2 (1.0 M Et_2O solution) was added dropwise via syringe. After 5 h of stirring, ^{11}B NMR analysis of the reaction mixture indicated that no reaction had occurred. Likewise, protonation was not observed following the addition, at 0 °C, of ∼10 drops of 18 M H_2SO_4 to a solution containing 0.20 g (0.44 mmol) of **PSH$^+$2$^-$** in 5 mL of CH_2Cl_2.

***endo*-6-(NCCH$_2$CH$_2$)-*arachno*-6,8-C$_2$B$_7$H$_{12}$ (3).** A 100-mL, two-neck, round-bottom flask equipped with a vacuum adapter, stirbar, and septum was charged with 0.34 g (3.0 mmol) of *arachno*-6,8-$C_2B_7H_{13}$ under a N_2 flow. Following addition of 10 mL of DME, the solution was maintained at 0 °C while an excess (∼0.3 g, ∼13 mmol) of NaH was added through one neck of the flask under a N_2 flow. When both the bubbling ceased and ^{11}B NMR analysis indicated complete formation of *arachno*-6,8-$C_2B_7H_{12}^-$ (**1**$^-$), the reaction was brought to room temperature and filtered in the glovebag to remove any excess NaH. The reaction solution was maintained at 0 °C while 1.0 mL (15.2 mmol) of acrylonitrile was added dropwise via syringe. The reaction mixture was placed in a 50 °C oil bath and covered with foil to exclude light. After stirring for 12 h, ^{11}B NMR analysis of the reaction mixture showed complete conversion to *endo*-6-(NCCH$_2$CH$_2$)-*arachno*-6,8-$C_2B_7H_{11}^-$ (**3**$^-$). The reaction flask was maintained at 0 °C while 3 mL of HCl−OEt_2 (1.0 M Et_2O solution) was added dropwise via syringe with stirring. The reaction mixture was brought to room temperature and then filtered in a glovebag to remove precipitated NaCl. The reaction solid was washed with 5 mL of DME, and the volatiles were removed from the filtrate under reduced pressure. Drying of the resulting residue on the high-vacuum line overnight afforded 0.49 g (3.0 mmol, 100%) of a white, powdery solid identified as *endo*-6-(NCCH$_2$CH$_2$)-*arachno*-6,8-$C_2B_7H_{12}$ (**3**): mp 60.0−61.0 °C. Anal. Calcd: C, 36.21; H, 9.72; N, 8.44. Found: C, 35.51; H, 9.51; N, 7.75. HRMS (CI+) (*m*/*e*) calcd for $^{12}C_5{}^{11}B_7{}^{14}N_1{}^1H_{17}$ (MH)$^+$ 168.2012, found 168.2019; IR (DRIFT, KBr, cm^{-1}) 3214 (s), 3039 (m), 2971 (m), 2578 (vs), 2250 (s), 2009 (m), 1456 (w), 1349 (w), 1263 (w), 1043 (m), 937 (w), 877 (m), 792 (m), 685 (w), 652 (w), 552 (m).

***exo*-6-(NCCH$_2$CH$_2$)-*arachno*-6,8-C$_2$B$_7$H$_{12}$ (4).** A 100-mL, two-neck, round-bottom flask equipped with a vacuum adapter and a stirbar was charged with 0.17 g (1.0 mmol) of *endo*-6-(NCCH$_2$CH$_2$)-*arachno*-6,8-$C_2B_7H_{12}$ (**3**). The flask was then degassed on the high-vacuum line, and 10 mL of THF was vacuum distilled into the flask at −196 °C. After thawing, a reflux condenser was attached to the flask, and the reaction mixture was then placed into a 50 °C oil bath to stir under a N_2 atmosphere. After 64 h, ^{11}B NMR analysis of the reaction mixture confirmed complete isomerization to *exo*-6-(NCCH$_2$CH$_2$)-*arachno*-6,8-$C_2B_7H_{12}$ (**4**). The flask was then brought to room temperature and filtered in the glovebag to remove any insoluble material. Removal of the volatiles from the filtrate under reduced pressure and subsequent drying of the residue overnight on the high-vacuum line afforded 0.16 g (0.97 mmol, 97%) of *exo*-6-(NCCH$_2$CH$_2$)-*arachno*-6,8-$C_2B_7H_{12}$ (**4**): mp 77.0−78.0 °C. Anal. Calcd: C, 36.21; H, 9.72; N, 8.44. Found: C, 35.41; H, 9.50; N, 5.64. HRMS (CI+) (*m*/*e*) calcd for $^{12}C_5{}^{11}B_7{}^{14}N_1{}^1H_{17}$ (MH)$^+$ 168.2012, found 168.2024; IR (CCl_4 sol, KBr plates, cm^{-1}) 3040 (w), 2950 (s), 2920 (m), 2870 (w), 2560 (vs), 2320 (w), 2250 (m), 2020 (w), 1450 (w), 1415 (w), 1385 (w), 1350 (w), 1260 (s), 1220 (w), 1080 (m), 1060 (m), 1020 (m), 940 (w), 905 (w), 880 (w), 710 (w), 680 (w).

Deprotonation of **4** was achieved by the addition of 0.32 g (1.5 mmol) of proton sponge to a stirred solution containing 0.12 g (0.7 mmol) of **4** dissolved in 5 mL of THF. Formation of **4**$^-$ was confirmed through a comparison of the experimental ^{11}B NMR chemical shifts with DFT/GIAO calculated shifts for the optimized geometry **IV**$^-$.

Attempted Isomerization of *endo*-6-(NCCH$_2$CH$_2$)-*arachno*-6,8-C$_2$B$_7$H$_{11}^-$ (3$^-$). To a 100-mL, two-neck, round-bottomed flask equipped with a vacuum adapter and a stirbar was added 0.17 g (1.0 mmol) of *endo*-6-(NCCH$_2$CH$_2$)-*arachno*-6,8-$C_2B_7H_{12}$ (**3**). The flask was degassed on the high-vacuum line, and 5 mL of THF was then vacuum distilled into the flask at −196 °C. After thawing, the flask was attached to the Schlenk line, and while the stirred solution was maintained at 0 °C, excess (∼0.1 g, ∼4 mmol) of NaH was added through one neck of the flask. The reaction was monitored by ^{11}B NMR spectroscopy until complete formation of **3**$^-$ was confirmed. The solution was filtered in the glovebag to remove excess NaH, and then, a reflux condenser was attached to the flask under a N_2 flow. After stirring for 15 h at 50 °C, ^{11}B NMR analysis of the reaction mixture indicated that no reaction had occurred.

$\mu_{6,9}$-(CH$_2$CH$_2$)-*arachno*-5,6,9-C$_3$B$_7$H$_{11}$ (5). A 0.25 g (1.5 mmol) sample of *endo*-6-(NCCH$_2$CH$_2$)-*arachno*-6,8-$C_2B_7H_{12}$ was dissolved in 10 mL of THF, and then, 0.014 g (1.7 mmol) of LiH was added while the solution was maintained at 0 °C. After the bubbling ceased and the formation of the *endo*-6-(NCCH$_2$CH$_2$)-*arachno*-6,8-$C_2B_7H_{11}^-$ (**3**$^-$) anion was confirmed by ^{11}B NMR spectroscopy, 1.0 mL of HCl−OEt_2 (1.0 M Et_2O solution) was added at −78 °C to partially regenerate the neutral *endo*-6-(NCCH$_2$CH$_2$)-*arachno*-6,8-$C_2B_7H_{12}$ (**3**). The mixture was then refluxed for 16 h at ∼70 °C under an inert atmosphere. After the mixture was filtered, the volatiles were vacuum evaporated on the high-vacuum line. The crude product was purified using flash silica gel chromatography using hexanes/CH_2Cl_2 cosolvent (3:1, v/v) to isolate 0.037 g (0.25 mmol, 17%) of white solid **5**. Compound **5** slowly sublimed at room temperature. Anal. Calcd: C, 39.81; H, 10.02. Found: C, 39.76; H, 10.42. LRMS (CI+) (*m*/*e*) calcd for $^{12}C_5{}^1H_{16}{}^{11}B_7$ (MH$^+$) 153, found 153 (seven boron pattern); IR (CH_2Cl_2, NaCl plates, cm^{-1}) 3050 (m), 2550 (s), 1150 (s), 1050 (s), 960 (m).

Crystallographic Data for PSH$^+$2$^-$ and 3. Pale-yellow crystals of PSH$^+$*endo*-6-*endo*-7-[μ_2-(C(CN)$_2$)$_2$]-*arachno*-6,8-$C_2B_7H_{12}^-$ (**PSH$^+$2$^-$**, UPenn #3145) were grown by slow evaporation of a heptane/CH_2Cl_2 solution at room temperature in air. Colorless crystals of *endo*-6-(NCCH$_2$CH$_2$)-*arachno*-6,8-$C_2B_7H_{12}$ (**3**, Upenn #3146) were grown by slow evaporation of a CH_2Cl_2 solution at −25 °C inside of a drybox.

Collection and Reduction of the Data. X-ray intensity data were collected on a Rigaku R-AXIS IIc area detector employing graphite-monochromated Mo Kα radiation (λ = 0.71069 Å) at a temperature of 296 K. Indexing for **PSH$^+$2$^-$** and **3** were performed from a series of 1° oscillation images with exposures of 200 s (**PSH$^+$2$^-$**) and 480 s (**3**) per frame. Hemispheres of data were collected using 6° (**PSH$^+$2$^-$**) and 5° (**3**) oscillation angles with exposures of 150 s (**PSH$^+$2$^-$**) and 1800 s (**3**) per frame. Crystal-to-detector distances were 82 mm. Oscillation images were processed using bioteX,[4] producing a listing of unaveraged F^2 and $\sigma(F^2)$ values which were then passed to the teXsan[5] program package for further processing and structure solution on a Silicon Graphics Indigo R4000 computer. The intensity data were corrected for Lorentz and polarization effects, but not for absorption.

Solution and Refinement of the Structures. The structures were solved by direct methods (SIR92).[6] Refinement was by full-matrix

(4) *bioteX: A suite of programs for the Collection, Reduction and Interpretation of Imaging Plate Data*; Molecular Structure Corporation: The Woodlands, TX, 1995.

(5) *teXsan: Crystal Structure Analysis Program*; Molecular Structure Corporation: The Woodlands, TX, 1985 and 1992.

Table 2. Crystallographic Data for PSH^+*endo*-6-*endo*-7-[μ_2-$(C(CN)_2)_2$]-*arachno*-6,8-$C_2B_7H_{12}^-$ (**PSH$^+$2$^-$**) and *endo*-6-$(NCCH_2CH_2)$-*arachno*-6,8-$C_2B_7H_{12}$ (**3**)

	PSH$^+$2$^-$	**3**
formula	$C_{22}B_7H_{31}N_6$	$C_5B_7H_{16}N$
fw	455.20	165.86
cryst class	triclinic	triclinic
space group	$P\bar{1}$ (#2)	$P\bar{1}$ (#2)
Z	2	4
cell constants		
a	12.6782(3)Å	11.7236(11)Å
b	12.8430(3)Å	13.6056(8)Å
c	9.4842(2)Å	7.0390(6)Å
α	90.3710(10)°	92.360(5)°
β	109.8320(10)°	102.756(4)°
γ	113.223(2)°	87.387(6)°
V	1317.30(5)Å^3	1093.4(2)Å^3
μ	0.66 cm^{-1}	0.49 cm^{-1}
cryst size, mm^3	0.54 × 0.50 × 0.35	0.32 × 0.30 × 0.08
D_{calcd}	1.148 g/cm^3	1.008 g/cm^3
F(000)	480	352
radiation	Mo Kα (λ = 0.71069 Å)	Mo Kα (λ = 0.71069 Å)
2θ range	5.32−50.7°	5.94−50.68°
hkl collected	$-15 \le h \le 15$ $-15 \le k \le 15$ $-11 \le l \le 11$	$-14 \le h \le 14$ $-16 \le k \le 16$ $-8 \le l \le 8$
no. reflns measured	10742	7830
no. unique reflns	4410 (R_{int} = 0.0201)	3571 (R_{int} = 0.0254)
no. obsd reflns	3946 ($F > 4\sigma$)	2801 ($F > 4\sigma$)
no. reflns used in refinement	4410	3571
no. params	441	236
R indices ($F > 4\sigma$)	R1 = 0.0485 wR2 = 0.1146	R1 = 0.0866 wR2 = 0.2338
R indices (all data)	R1 = 0.0547 wR2 = 0.1188	R1 = 0.1075 wR2 = 0.2555
GOF	1.111	1.119
final difference peaks, e/Å^3	+0.161, −0.113	+0.343, −0.187

least -squares based on F^2 using SHELXL-93.[7] All reflections were used during refinement (F^2's that were experimentally negative were replaced by $F^2 = 0$). The weighting schemes were $w = 1/[\sigma^2(F_o^2)+ 0.0472P^2 + 1.2719P]$ (**PSH$^+$2$^-$**) and $w = 1/[\sigma^2(F_o^2) + 0.1113P^2 + 0.4633P]$ (**3**) where *P* is $(F_o^2+ 2F_c^2)/3$. Non-hydrogen atoms were refined anisotropically and hydrogen atoms were refined isotropically. Crystal and refinement data are given in Table 2.

Computational Studies. The DFT/GIAO/NMR method,[8] using either the Gaussian 94[9] or Gaussian 98[10] programs, was used in a manner similar to that previously described.[11−13] The geometries were fully optimized at the B3LYP/6-311G* level within the specified symmetry constraints (using the standard basis sets included) on a (2)-processor Origin 2000 computer running IRIX 6.5.5 or a (6)-processor Power Challenge XL computer running IRIX 6.5.6. A vibrational frequency analysis was carried out on each optimized geometry at the B3LYP/6-311G* level with a true minimum found for each structure (i.e., possessing no imaginary frequencies). The NMR chemical shifts were calculated at the B3LYP/6-311G* level using the GIAO option within Gaussian 94/98. ^{11}B NMR GIAO chemical shifts are referenced to BF_3-OEt_2 using an absolute shielding constant of 102.24.[13,14] The ^{13}C NMR GIAO chemical shifts are referenced to TMS using an absolute shielding constant of 184.38.

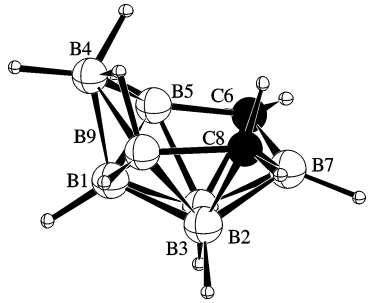

Figure 1. DFT optimized geometry (B3LYP/6-311G*) for *arachno*-6,8-$C_2B_7H_{12}^-$ (**I$^-$**).

Results and Discussion

Structure of the *arachno*-6,8-$C_2B_7H_{12}^-$ (1$^-$) Anion. Mono-deprotonation of the neutral *arachno*-6,8-$C_2B_7H_{13}$ carborane could, in principle, result in removal of either a bridge or an *endo*-CH proton. Previous deuterium-exchange studies[15] of *exo*-6-CH_3-*arachno*-6,8-$C_2B_7H_{12}$ and *exo*-6-*exo*-8-$(CH_3)_2$-*arachno*-6,8-$C_2B_7H_{11}$, as well as reactivity studies[1] of the *arachno*-6,8-$C_2B_7H_{12}^-$ (**1$^-$**) anion, are consistent with deprotonation at an *endo*-CH. In agreement with these earlier observations, our DFT/GIAO computational studies of *arachno*-6,8-$C_2B_7H_{12}^-$ now show that the chemical shifts and assignments calculated for the optimized geometry **I$^-$** in Figure 1, in which one of the *endo*-protons has been removed, agree well with the experimental ^{11}B NMR spectrum observed for **1$^-$**. This structure is, in fact, 11.0 kcal/mol lower in energy than a bridge-deprotonated structure. Consistent with our earlier studies[1] that demonstrated **1$^-$** is a good carbon-centered nucleophile that will readily add to polarized multiple-bonds, the calculations also show that the HOMO of **I$^-$** is largely localized as a lone pair at the *endo*-C6 position (Figure 2).

(6) SIR92: Altomare, A.; Burla, M. C.; Camalli, M.; Cascarano, M.; Giacovazzo, C.; Guagliardi, A.; Polidoro, G. *J. Appl. Crystallogr.* **1994**, *27*, 435.
(7) Sheldrick, G. M. *SHELXL-93: Program for the Refinement of Crystal Structures*; University of Göttingen: Göttingen, Germany 1993.
(8) Yang, X.; Jiao, H.; Schleyer, P. v. R. *Inorg. Chem.* **1997**, *36*, 4897−4899 and references therein.
(9) Frisch, M. J.; Trucks, G. W.; Schlegel, H. B.; Gill, P. M. W.; Johnson, B. G.; Robb, M. A.; Cheeseman, J. R.; Keith, T.; Petersson, G. A.; Montgomery, J. A.; Raghavachari, K.; Al-Laham, M. A.; Zakrzewski, V. G.; Ortiz, J. V.; Foresman, J. B.; Cioslowski, J.; Stefanov, B. B.; Nanayakkara, A.; Challacombe, M.; Peng, C. Y.; Ayala, P. Y.; Chen, W.; Wong, M. W.; Andres, J. L.; Replogle, E. S.; Gomperts, R.; Martin, R. L.; Fox, D. J.; Binkley, J. S.; Defrees, D. J.; Baker, J.; Stewart, J. P.; Head-Gordon, M.; Gonzalez, C.; Pople, J. A. *Gaussian 94*, revision E.2; Gaussian, Inc.: Pittsburgh, PA, 1995.
(10) Frisch, M. J.; Trucks, G. W.; Schlegel, H. B.; Scuseria, G. E.; Robb, M. A.; Cheeseman, J. R.; Zakrzewski, V. G.; Montgomery, J. A., Jr.; Stratmann, R. E.; Burant, J. C.; Dapprich, S.; Millam, J. M.; Daniels, A. D.; Kudin, K. N.; Strain, M. C.; Farkas, O.; Tomasi, J.; Barone, V.; Cossi, M.; Cammi, R.; Mennucci, B.; Pomelli, C.; Adamo, C.; Clifford, S.; Ochterski, J.; Petersson, G. A.; Ayala, P. Y.; Cui, Q.; Morokuma, K.; Malick, D. K.; Rabuck, A. D.; Raghavachari, K.; Foresman, J. B.; Cioslowski, J.; Ortiz, J. V.; Stefanov, B. B.; Liu, G.; Liashenko, A.; Piskorz, P.; Komaromi, I.; Gomperts, R.; Martin, R. L.; Fox, D. J.; Keith, T.; Al-Laham, M. A.; Peng, C. Y.; Nanayakkara, A.; Gonzalez, C.; Challacombe, M.; Gill, P. M. W.; Johnson, B. G.; Chen, W.; Wong, M. W.; Andres, J. L.; Head-Gordon, M.; Replogle, E. S.; Pople, J. A. *Gaussian 98*, revision A.9; Gaussian, Inc.: Pittsburgh, PA, 1998.
(11) Keller, W.; Barnum, B. A.; Bausch, J. W.; Sneddon, L. G. *Inorg. Chem.* **1993**, *32*, 5058−5066.
(12) Bausch, J. W.; Rizzo, R. C.; Sneddon, L. G.; Wille, A. E.; Williams, R. E. *Inorg. Chem.* **1996**, *35*, 131−135.
(13) Tebben, A. J. Master's Thesis, Villanova University, 1997.
(14) Tebben, A. J.; Bausch, J. W. Private communication.
(15) Tebbe, F. N.; Garrett, P. M.; Hawthorne, M. F. *J. Am. Chem. Soc.* **1968**, *90*, 869−879.

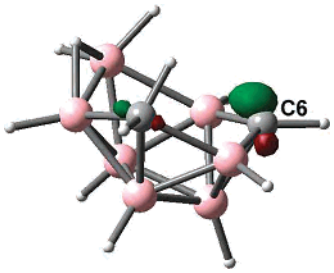

Figure 2. HOMO density surface (B3LYP/6-311G*) for *arachno*-6,8-$C_2B_7H_{12}^-$ (**I**$^-$).

Reactions of 1$^-$ with Tetracyanoethylene and Acrylonitrile. The reaction of PSH^+*arachno*-6,8-$C_2B_7H_{12}^-$ (**PSH$^+$1$^-$**) with the activated olefin tetracyanoethylene (TCNE) yields PSH^+*endo*-6-*endo*-7-[μ_2-$(C(CN)_2)_2$]-*arachno*-6,8-$C_2B_7H_{12}^-$ (**PSH$^+$2$^-$**) in moderate yield (eq 1). The product was isolated as an air-stable, yellow solid having a composition established by both high-resolution mass spectrometry and a crystallographic determination. Attempts to acidify **PSH$^+$2$^-$** by either the in situ addition of HCl−OEt_2 or a two-phase CH_2Cl_2/H_2SO_4 method were unsuccessful.

$$\underset{\textbf{PSH}^+\textbf{1}^-}{PSH^+\textit{arachno}\text{-}6,8\text{-}C_2B_7H_{12}^-} + \underset{\text{TCNE}}{(NC)_2C{=}C(CN)_2} \xrightarrow[\text{DME}]{} \underset{\textbf{PSH}^+\textbf{2}^-}{PSH^+\textit{endo}\text{-}6\text{-}\textit{endo}\text{-}7\text{-}[\mu_2\text{-}(C(CN)_2)_2]\text{-}\textit{arachno}\text{-}6,8\text{-}C_2B_7H_{12}^-} \quad (1)$$

The single-crystal X-ray crystallographic study showed that the TCNE fragment in **PSH$^+$2$^-$** is bonded in a bridging fashion across the C6−B7 edge of the cluster (Figure 3a). This geometry is consistent with cycloaddition of the TCNE to the carborane framework resulting in the breaking of the C6−B7 bond (2.790(2) Å) with concurrent formation of the C6−C10 (1.547(2) Å) and B7−C11 bonds (1.641(3) Å). Reduction of the TCNE double bond is evidenced both by the tetrahedral angles at C10 and C11 (e.g., C12−C10−C13, 106.0(1)°; C14−C11−C15, 109.2(2)°; C6−C10−C11, 105.4(1)°; B7−C11−C10 110.8(1)°) and by the longer C10−C11 bond (1.572(2) Å) compared to the C=C lengths found in the two crystal structure determinations of TCNE, 1.317(9) Å (monoclinic) and 1.344(3) Å (cubic).[16] The C10−C11 distance is also similar to those which have been found in other compounds including, for example, methyl-3,3,4,4-tetracyanoethyl-3,4-dihydro-5-isopropyl-2-(*p*-nitrophenyl)-2*H*-pyrrole-2-carboxylate (1.582(5) Å)[17] and $CpFe(CO)_2$-$CH_2CHC(CN)_2C(CN)_2CH_2CH{=}CH_2$ (1.574(6) Å),[18] resulting from TCNE cycloaddition. The torsional angles about the C10−C11 bond, 43.53(19)° (C12−C10−C11−C14) and 47.10(15)° (C13−C10−C11−C15), also indicate that the TCNE fragment is no longer planar.

The TCNE fragment in **2**$^-$ is probably best viewed as a classical exopolyhedral substituent bridging the C6 and B7 atoms of the open 9-vertex framework. The C_2B_7-fragment of the cluster would then be a 26 skeletal electron, 9-vertex *hypho*-system ($n + 4$ skeletal electron pairs) and should have a more open structure than that found for **1**$^-$. The TCNE addition has the effect of generating an open pentagonal ring containing three cluster atoms and two TCNE carbons (B2−C6−C10−C11−B7). In addition to the lengthened C6−B7 edge, the B2−B5 (2.051(3) Å) and B2−B7 (2.070(3) Å) lengths in **2**$^-$ are also significantly longer than those found in *arachno*-6,8-$C_2B_7H_{13}$ (**1**) (1.788(6) Å and 1.749(5) Å), while B2−C6 (1.603(3) Å) and B5−C6 (1.569(3) Å) in **2**$^-$ are shortened relative to those in **1** (1.668(4) Å and 1.706(5) Å).[19]

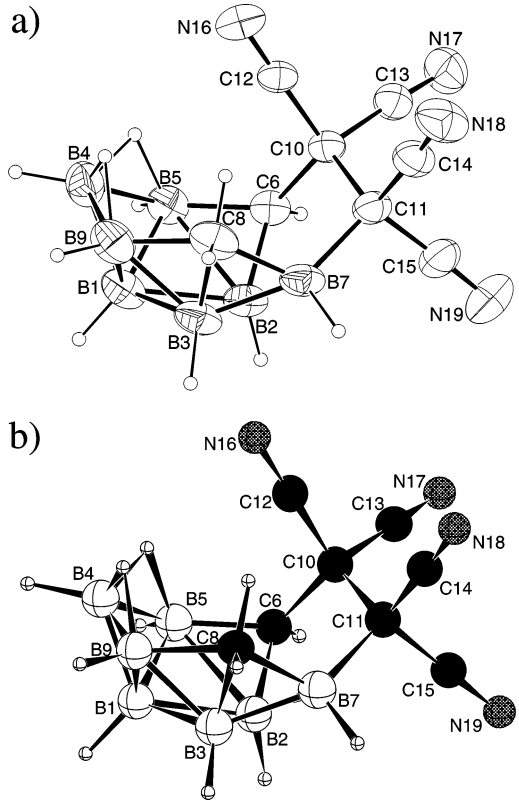

Figure 3. Comparison of the (a) crystallographically determined structure of the *endo*-6-*endo*-7-[μ_2-$(C(CN)_2)_2$]-*arachno*-6,8-$C_2B_7H_{12}^-$ anion in **PSH$^+$2$^-$** with that of (b) its DFT calculated geometry **II**$^-$. Selected bond lengths (Å) and angles (deg): **PSH$^+$2$^-$**, C10−C11, 1.572(2); B2−C6, 1.603(3); B5−C6, 1.569(3); B2−B5, 2.051(3); B2−B7, 2.070(3); C6−B7, 2.790(2); C6−C10, 1.547(2); B7−C11, 1.641(3); B7−C8, 1.696(3); C8−B9, 1.711(3); C12−C10−C11−C14, 43.53(19); C13−C10−C11−C15, 47.10(15); C6−C10−C11−B7, 42.34(14); **II**$^-$, C10−C11, 1.595; B2−C6, 1.613; B5−C6, 1.589; B2−B5, 2.075; B2−B7, 2.085; C6−B7, 2.811; C6−C10, 1.561; B7−C11, 1.669; B7−C8, 1.696; C8−B9, 1.714; C12−C10−C11−C14, 40.8; C13−C10−C11−C15, 45.1; C6−C10−C11−B7, 40.3.

In agreement with its crystallographically determined C_1 cage-symmetry, the ^{11}B NMR spectrum of **PSH$^+$2$^-$** contains seven doublets of equal intensity. In addition to the characteristic PSH^+ peaks, the ^{11}B-decoupled ^{1}H NMR spectrum contained seven terminal BH singlets, two separate bridging-hydrogen peaks, and three cage-carbon CH resonances, with the upfield shift (−0.91 ppm) of one of the CH resonances being highly characteristic of an *endo*-hydrogen. The ^{1}H-decoupled ^{13}C NMR spectrum contained peaks for the TCNE

(16) (a) Dhar, D. N. *Chem. Rev.* **1967**, *67*, 611−622. (b) Little, R. G.; Pautler, D.; Coppens, P. *Acta Crystallogr.* **1971**, *B27*, 1493−1499.
(17) Ibata, T.; Isogami, Y.; Nakawa, H.; Tamura, H.; Suga, H.; Shi, X.; Fujieda, H. *Bull. Chem. Soc. Jpn.* **1992**, *65*, 1771−1778.
(18) Lee, G. H.; Peng, S. M.; Lush, S. F.; Mu, D.; Liu, R. S. *Organometallics* **1988**, *7*, 1155−1161.
(19) Voet, D.; Lipscomb, W. N. *Inorg. Chem.* **1967**, *6*, 113−119.

and PSH^+ fragments, along with two broad cage-carbon resonances. The DFT calculated distances and angles, as well as the GIAO calculated ^{11}B and ^{13}C NMR chemical shifts and assignments, for the optimized geometry **II**$^-$ given in Figure 3b, are in excellent agreement with the experimentally observed values for **2**$^-$.

The reaction of **1**$^-$ with acrylonitrile resulted in the exclusive formation of *endo*-6-($NCCH_2CH_2$)-*arachno*-6,8-$C_2B_7H_{12}$ (**3**$^-$). The anion was then acidified in situ by the addition of $HCl-OEt_2$ to afford *endo*-6-($NCCH_2CH_2$)-*arachno*-6,8-$C_2B_7H_{12}$ (**3**) in high yield (eq 2).

$$\underset{\mathbf{1}^-}{\textit{arachno}\text{-}6,8\text{-}C_2B_7H_{12}} + NC(H)C{=}CH_2 \xrightarrow[2.\ H^+]{1.\ \Delta} \underset{\mathbf{3}}{\textit{endo}\text{-}6\text{-}(NCCH_2CH_2)\text{-}\textit{arachno}\text{-}6,8\text{-}C_2B_7H_{12}} \quad (2)$$

Compound **3** was isolated as a slightly air-sensitive, white solid. Although the elemental analyses of **3** were slightly out of the normal range, its composition was established by both high-resolution mass spectrometry and a crystallographic determination.

The previously known monomethyl-, dimethyl-, and diphenyl- C6-substituted derivatives of *arachno*-6,8-$C_2B_7H_{13}$ that were prepared by the chromic acid mediated oxidation/degradation of the corresponding 11-vertex *nido*-$R_2C_2B_9H_{11}$ derivatives have all exhibited *exo*-substitutions,[15,19] but the single-crystal X-ray crystallographic study confirmed that in **3** the cyanoethyl fragment is bound at the *endo*-position of the C6 cage-carbon (Figure 4).

For **3**, there are two independent molecules in the unit cell that, as shown by the different torsional angles for their B5−C6−C10−C11 bonds (183.80(27)° versus 292.06(33)°), differ only in the conformations of their ($NCCH_2CH_2$)-fragments. The B2−C6 bond lengths in the two conformers of **3** (1.727(5) and 1.715(6) Å) are significantly longer than the B3−C8 lengths (1.655(5) and 1.661(6) Å), as well as longer than that observed in the parent *arachno*-6,8-$C_2B_7H_{13}$ (1.668(4) Å). Likewise, the C10−C6−C8 angles (91.7° and 88.5°) are much larger than the *endo*-C8H−C8−C6 angles (72.5° and 74.7°). These distance and angle differences most likely result from the larger steric requirements of the *endo*-cyanoethyl group compared to the *endo*-C8H. Indeed, in both conformers one of the cyanoethyl methylene hydrogens is found to be less than the van der Waals radii away from the *endo*-C8H (1.993 and 1.995 Å). The C10−C11 bond lengths (1.507(5) and 1.527(4) Å) in **3** are consistent with reduction of the acrylonitrile C═C bond to a single bond.

The ^{11}B NMR spectrum of **3** differs from that of the parent in that, owing to its lower C_1 symmetry, there are now seven equal-intensity doublets. The ^{11}B-decoupled ^1H NMR spectrum contains, in addition to the cyanoethyl resonances, seven terminal-BH singlets and two nonequivalent bridging-hydrogen peaks, along with one upfield (−0.44 ppm) *endo*-CH resonance and two lower field *exo*-CH resonances. The ^1H-decoupled ^{13}C NMR spectrum contains the expected three sharp peaks of $NCCH_2CH_2$-carbons and two broad cage-carbon resonances.

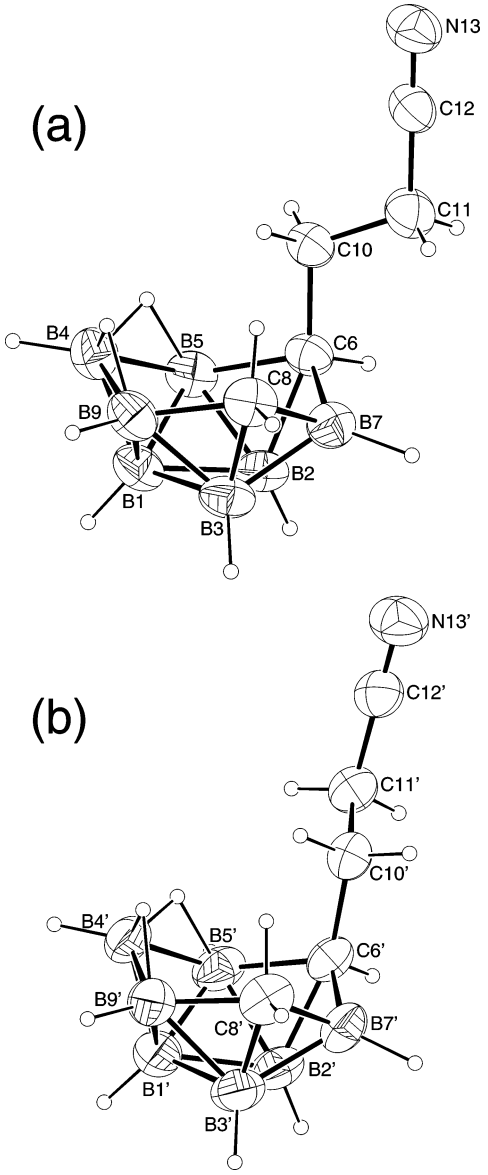

Figure 4. ORTEP representations of the two independent molecules in the unit cell of *endo*-6-($NCCH_2CH_2$)-*arachno*-6,8-$C_2B_7H_{12}$ (**3**). Selected bond lengths (Å) and angles (deg): (a) C6−C10, 1.549(4); C10−C11, 1.507(5); C11−C12, 1.470(5); C12−N13, 1.131(4); C6−B2, 1.727(5); C8−B3, 1.655(5); C6−B7, 1.689(5); B7−C8, 1.690(5); C8−B9, 1.711(5); B9−B4, 1.798(6); B4−B5, 1.813(6); B5−C6, 1.748(5); C8−C6−C10, 91.7(2); C6−C8−*endo*-C8H, 72.5; B5−C6−C10−C11, 183.80(27); (b) C6′−C10′, 1.554(4); C10′−C11′, 1.526(4); C11′−C12′, 1.460(5); C12′−N13′, 1.120(4); C6′−B2′, 1.715(6); C8′−B3′, 1.661(6); C6′−B7′, 1.714(5); B7′−C8′, 1.706(6); C8′−B9′, 1.730(6); B9′−B4′, 1.788(7); B4′−B5′, 1.778(7); B5′−C6′, 1.694(5); C8′−C6′−C10′, 88.5(2); C6′−C8′−*endo*-C8H′, 74.7; B5′−C6′−C10′−C11′, 292.06(33).

DFT calculations on the two conformers observed in the crystallographic determination of **3** yielded optimized geometries **IIIa** and **IIIb** (Figure 5) that differ by only 0.4 kcal/mol. The GIAO calculated ^{11}B and ^{13}C NMR shifts for the two conformers are slightly different. However, consistent with a freely rotating cyanoethyl group in solution, the average of the calculated chemical shifts for the two conformers is in excellent agreement with the ^{11}B NMR shift values observed for **3**. The DFT calculated distances and angles agree with the trends noted above in the values observed in the crystallographic determination of **3**.

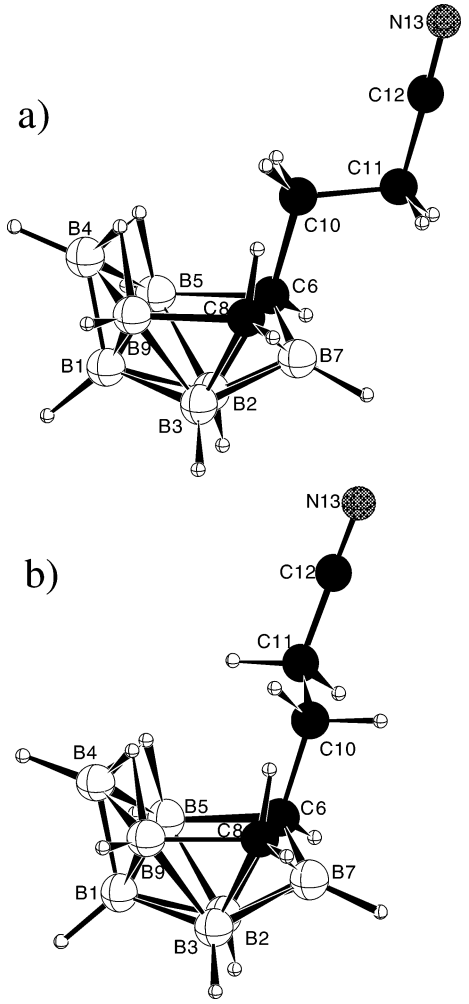

Figure 5. DFT optimized geometries for the two conformers of *endo*-6-($NCCH_2CH_2$)-*arachno*-6,8-$C_2B_7H_{12}$ (**IIIa** and **IIIb**). Selected calculated bond lengths (Å) and angles (deg): (a) C6−C10, 1.557; C10−C11, 1.544; C11−C12, 1.461; C12−N13, 1.153; C6−B2, 1.743; C8−B3, 1.671; C6−B7, 1.690; B7−C8, 1.694; C8−B9, 1.726; B9−B4, 1.830; B4−B5, 1.831; B5−C6, 1.753; C10−C6−*exo*-C6H, 104.9; *endo*-C8H−C8−*exo*-C8H, 109.8; C8−C6−C10, 91.4; C6−C8−*endo*-C8H, 73.1; B5−C6−C10−C11, 183.8; (b) C6′−C10′, 1.559; C10′−C11′, 1.545; C11′−C12′, 1.461; C12′−N13′, 1.153; C6′−B2′, 1.742; C8′−B3′, 1.671; C6′−B7′, 1.708; B7′−C8′, 1.697; C8′−B9′, 1.715; B9′−B4′, 1.831; B4′−B5′, 1.838; B5′−C6′, 1.730; C10′−C6′−CH6′, 105.0; H8a′−C8′−H8b′, 109.7; C8′−C6′−C10′, 89.4; C6′−C8′−*endo*-C8H′, 73.7; B5′−C6′−C10′−C11′, 290.1.

The reactions of $\mathbf{1}^-$ with tetracyanoethylene and acrylonitrile can be envisioned to occur by mechanistic pathways similar to that previously proposed for the reactions of $\mathbf{1}^-$ with polar acetylenes.[1c] Thus, as shown in Figure 6, the initial step in both reactions should be nucleophilic attack of the $\mathbf{1}^-$ anion at the activated olefin to yield an *endo*-substituted carborane anion (**A** and **B**) having the negative charge localized on the substituent. The resulting electrophilic fragment can then react with the cage in at least two different ways. In the case of the TCNE reaction (Figure 6a), the substituent further condenses with attack at the most electropositive cage-boron, B7,[20] resulting in addition of the TCNE across the C6−B7 edge. This process can be considered analogous to the well-known cycloaddition of TCNE to dienes and carbenes.[21]

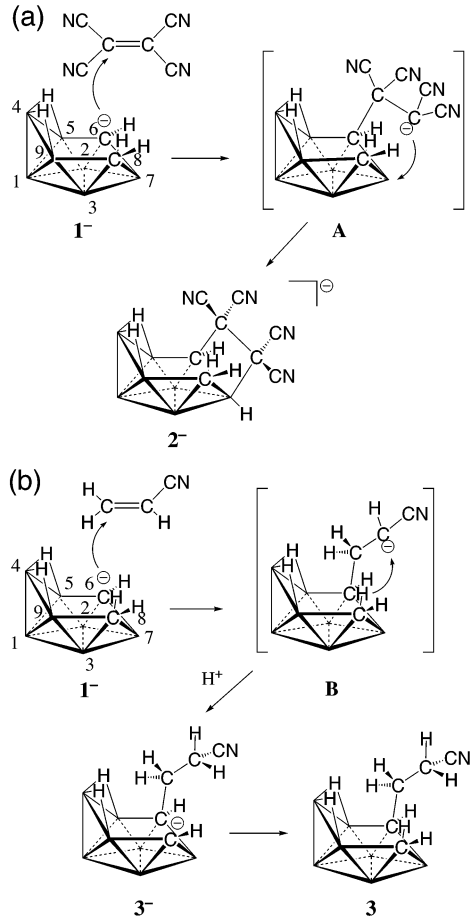

Figure 6. Possible reaction steps in the formation of *endo*-6-*endo*-7-[μ_2-$(C(CN)_2)_2$]-*arachno*-6,8-$C_2B_7H_{12}^-$ ($\mathbf{2}^-$) and *endo*-6-($NCCH_2CH_2$)-*arachno*-6,8-$C_2B_7H_{12}$ (**3**) from $\mathbf{1}^-$.

In the acrylonitrile reaction, initial nucleophilic attack at the activated β-carbon would generate structure **B** having the negative charge localized on the cyanoethyl α-carbon (Figure 6b). Rather than adding to the cage, this anion abstracts a cage-proton to generate $\mathbf{3}^-$. DFT optimized geometries for three possible structures of $\mathbf{3}^-$, where the abstracted proton comes from the *endo*-C8H or one of the two bridging-hydrogens, are illustrated in Figure 7. Structure $\mathbf{IIIa}^-$, resulting from *endo*-C8H proton transfer, is energetically favored over isomers, $\mathbf{IIIb}^-$ and $\mathbf{IIIc}^-$, and the GIAO calculated ^{11}B and ^{13}C chemical shifts for this isomer are in good agreement with those observed experimentally. The structure and ^{11}B NMR chemical shifts of $\mathbf{3}^-$ are also similar to that of 6-(NCCH═CH)-*arachno*-6,8-$C_2B_7H_{12}^-$ which was reported to be formed during the reaction of $\mathbf{1}^-$ with cyanoacetylene.[1c]

When the acrylonitrile reaction was monitored by ^{11}B NMR spectroscopy, only $\mathbf{1}^-$ and $\mathbf{3}^-$ were observed without any other intermediates. Thus, proton transfer must be fast or occur concertedly with the acrylonitrile addition. This intramolecular hydrogen-transfer reaction can be considered

(20) Dolansky, J.; Hermanek, S.; Zahradnik R. *Collect. Czech. Chem. Commun.* **1981**, *46*, 2479.
(21) Ciganek, E.; Linn, W. J.; Webster, O. W. In *The Chemistry of the Cyano Group*; Rappoport, Z., Ed.; Wiley-Interscience: New York, 1970; pp 446−474.

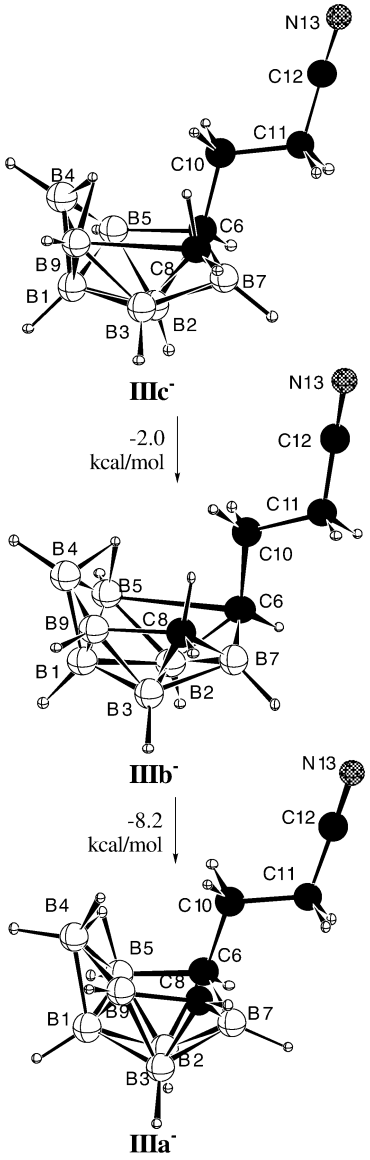

Figure 7. DFT optimized geometries for *endo*-6-($NCCH_2CH_2$)-*arachno*-6,8-$C_2B_7H_{11}^-$ (**IIIa**−**c**$^-$), selected bond lengths (Å) and angles (deg): **IIIa**$^-$, C10−C11, 1.547; C6−C10, 1.545; C8−B9, 1.530; B3−C8, 1.667; B3−B9, 1.813; B4−B9, 1.987; B4−B5, 1.895; B7−C8, 1.552; B5−C6, 1.672; H6a−C6−C10, 107.2; C6−B7−C8, 113.0; B5−C6−C10−C11, 180.8; **IIIb**$^-$, C10−C11, 1.551; C6−C10, 1.524; C8−B9, 1.744; B3−C8, 1.678; B3−B9, 1.776; B4−B9, 1.697; B4−B5, 1.712; B7−C8, 1.701; B5−C6, 2.647; H6a−C6−C10, 107.7; C6−B7−C8, 115.4; B5−C6−C10−C11, 179.3; **IIIc**$^-$, C10−C11, 1.549; C6−C10, 1.545; C8−B9, 2.355; B3−C8, 1.687; B3−B9, 1.806; B4−B9, 1.743; B4−B5, 1.686; B7−C8, 1.572; B5−C6, 1.756; H6a−C6−C10, 106.2; C6−B7−C8, 114.3; B5−C6−C10−C11, 183.5.

analogous to the well-known [1,5] sigmatropic rearrangement *ene*-reaction.

Isomerization of 3 to *exo*-6-($NCCH_2CH_2$)-*arachno*-6,8-$C_2B_7H_{12}$ (4). Heating **3** in THF at 50 °C for 64 h resulted in the isomerization of the cyanoethyl fragment from the *endo* to the *exo* C6-position to afford *exo*-6-($NCCH_2CH_2$)-*arachno*-6,8-$C_2B_7H_{12}$ (**4**) in high-yield (eq 3).

$$\underset{\mathbf{3}}{\textit{endo}\text{-6-}(NCCH_2CH_2)\text{-}\textit{arachno}\text{-6,8-}C_2B_7H_{12}} \xrightarrow[50\ ^\circ C]{THF} \underset{\mathbf{4}}{\textit{exo}\text{-6-}(NCCH_2CH_2)\text{-}\textit{arachno}\text{-6,8-}C_2B_7H_{12}} \quad (3)$$

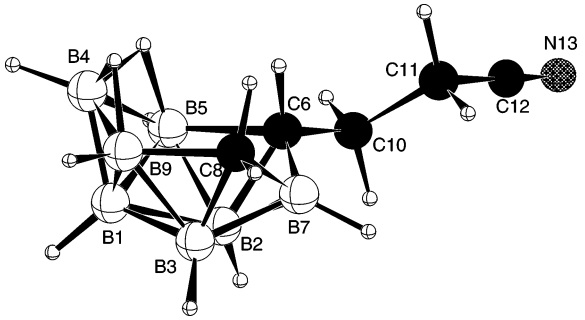

Figure 8. DFT optimized geometry for *exo*-6-($NCCH_2CH_2$)-*arachno*-6,8-$C_2B_7H_{12}$ (**IV**), selected bond lengths (Å) and angles (deg): B2−C6, 1.685; B3−C8, 1.682; C6−B7, 1.694; B7−C8, 1.704; C8−B9, 1.719; B9−B4, 1.836; B4−B5, 1.833; B5−C6, 1.762; C6−C10, 1.531; C10−C11, 1.543; C11−C12, 1.461; C12−N13, 1.153; C10−C6−H6, 110.7; H8a−C8−H8b, 109.6; *endo*-C6H−C6−C8, 70.8; *endo*-C8H−C8−C6, 73.7; B5−C6−C10−C11, 147.6.

The product was isolated as a slightly air-sensitive, white solid. Its composition was determined by high-resolution mass spectrometry. The ^{11}B, ^{13}C, and ^1H NMR data for **4** are similar to those observed for **3**, with the exception that in its ^1H NMR spectrum two of the three cage-CH resonances of **4** have upfield peaks (−0.49 and −0.58 ppm) characteristic of *endo*-CH cage hydrogens and only one in the lower field (0.33 ppm) *exo*-CH cage region. The DFT optimized structure **IV** is shown in Figure 8. The calculated C10−C11 (1.543 Å) and C6−C10 (1.531 Å) bond lengths are consistent with C−C single bonds. The similar H6−C6−C10 (110.7°) and H8a−C8−H8b (109.6°) angles and B2−C6 (1.686 Å) and B3−C8 (1.682 Å) bond lengths show that *exo*-subsitution has little effect on the geometry about the cage-carbons. A comparison of the DFT/GIAO calculated chemical shifts for **IV** with those experimentally observed for **4** shows good agreement.

The DFT computations also showed that the *exo*-configuration isomer **IV** is 7.7 kcal/mol more stable than *endo*-isomer **IIIa** and 8.1 kcal/mol more stable than **IIIb**. Therefore, **3** is a kinetic product resulting from initial addition to **1**$^-$ which, upon heating, then rearranges to the more stable *exo*-isomer **4**. This is the first reported example of an *endo* to *exo* isomerization to be observed at a cage carbon atom in a carborane. Possible mechanisms of this unique isomerization process will be discussed in a separate publication.[22]

Synthesis of $\mu_{6,9}$-(CH_2CH_2)-*arachno*-5,6,9-$C_3B_7H_{11}$ (5). Although **3**$^-$ did not react upon heating, when it was heated in the presence of a small amount of **3**, it formed the ethylene-bridged 10-vertex tricarbaborane $\mu_{6,9}$-(CH_2CH_2)-*arachno*-5,6,9-$C_3B_7H_{11}$ (**5**) (eq 4).

$$\underset{\mathbf{3}}{\textit{endo}\text{-6-}(NCCH_2CH_2)\text{-}\textit{arachno}\text{-6,8-}C_2B_7H_{12}} \xrightarrow[\Delta,\ -\text{“N”}]{\text{(1) LiH (1.1 equiv)}\ \text{(2) HCl (0.7 equiv)}} \underset{\mathbf{5}}{\mu_{6,9}\text{-}(CH_2CH_2)\text{-}\textit{arachno}\text{-5,6,9-}C_3B_7H_{11}} \quad (4)$$

The composition of **5** was confirmed by elemental analysis and mass spectrometry. The spectral and computational

(22) Hong, D.; Kadlecek, D. E.; Sneddon, L. G. In preparation.

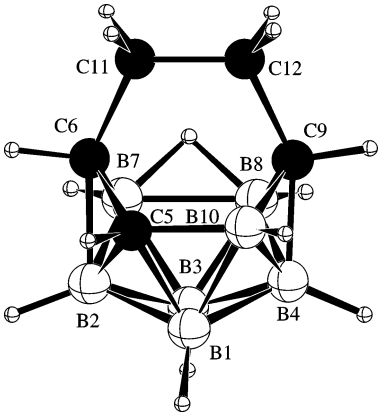

Figure 9. DFT optimized geometry for $\mu_{6,9}$-(CH_2CH_2)-*arachno*-5,6,9-$C_3B_7H_{11}$ (**V**), selected bond lengths (Å) and angles (deg): B7−B8, 1.879; C5−C6, 1.582; C6−C11, 1.555; C11−C12, 1.535; C9−C12, 1.572; C5−B10, 1.610; B2−C6, 1.797; B4−C9, 1.725; C6−C11−C12, 114.4; C9−C12−C11, 115.8; C6−C11−C12−C9, 359.1; B2−C6−C11−C12, 355.6; B4−C9−C12−C11, 0.5.

results support structure **V** shown in Figure 9. As can be seen in the figure, the nitrile carbon of the cyanoethyl group of $\mathbf{3}^-$ has inserted into the parent C_2B_7 framework at the C6 position in **5** to generate a 10-vertex tricarbaborane containing an ethylene bridge attached to the C6 and C9 carbons at their *endo*-positions. The 359.1° C6−C11−C12−C9 torsional angle in **V** confirms that the C11−C12 ethylene bridge lies in a vertical plane containing C6 and C9. The C6−C11−C12 (114.4°) and C9−C12−C11 (115.8°) bond angles and the C6−C11 (1.555 Å), C11−C12 (1.535 Å), and C9−C12 (1.572 Å) bond lengths are all indicative of a saturated system. All three cage-carbons are on the open face, and there is a single bridge-hydrogen at the B7−B8 edge. Supporting this structure, the ^{11}B NMR spectrum shows seven-boron resonances. In agreement with its GIAO assignment to the B7 boron, the peak at −14.2 ppm exhibits a doublet of doublets pattern characteristic of coupling with a terminal and one bridge-hydrogen. The other calculated ^{11}B chemical shift values for **V** are also in excellent agreement with the experimental data for **5**. The ^{1}H NMR spectrum showed the expected intensity-one bridge-hydrogen, three cage-CH, seven terminal-BH and two sharp intensity-two alkyl chain CH-resonances. In the ^{1}H-decoupled ^{13}C NMR spectrum, one of the three broad cage-carbon resonances exhibited a quartet structure owing to coupling to a single boron (J_{CB}, 35.9 Hz), which is in accord with its GIAO assignment to the C5 cage carbon that lies between C6 and B10.

If the C11 and C12 carbons are each considered to be a part of the cluster, then **5** could be categorized as a *hypho*-class compound with 32 skeletal electrons and 12 vertices.[23] However, the resonances observed for the $C(11)H_2$−$C(12)H_2$ fragment in the ^{13}C and ^{1}H NMR spectra are characteristic of an aliphatic chain. Thus, it would be more appropriate to view this unit as an exopolyhedral tether bridging the C6 and C9 cage-carbons at their *endo*-positions. The C_3B_7 cluster fragment in **5** would then be a 26 skeletal-electron *arachno*-system and would be predicted to have its observed structure, which is derived from an icosahedron by removing two vertices. Similar 6,9-bridging structures

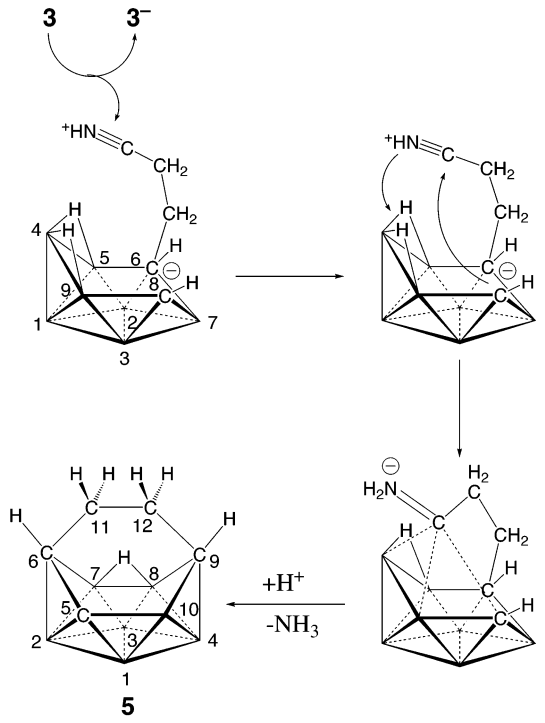

Figure 10. Proposed reaction sequence leading to the formation of $\mu_{6,9}$-(CH_2CH_2)-*arachno*-5,6,9-$C_3B_7H_{11}$.

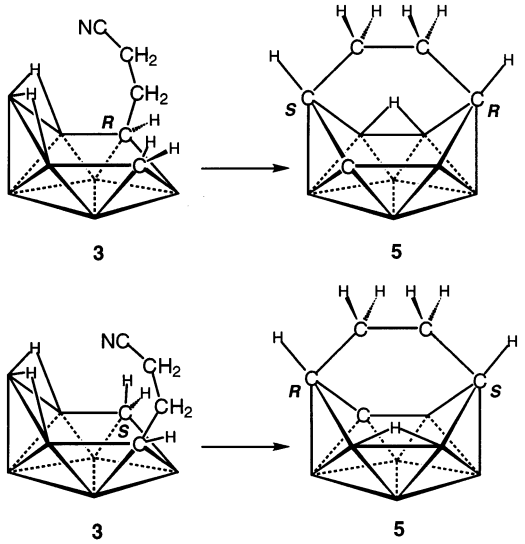

Figure 11. Illustration of the regio- and stereospecificity in the formation of $\mu_{6,9}$-(CH_2CH_2)-*arachno*-5,6,9-$C_3B_7H_{11}$.

have, in fact, been confirmed for several other 10-vertex *arachno*-clusters.[24]

It has been previously shown that the synthesis of the 6-CH_3-*nido*-5,6,9-$C_3B_7H_9^-$ tricarbaborane anion from the reaction of *arachno*-6,8-$C_2B_7H_{12}^-$ and CH_3CN requires the presence of a small amount of neutral *arachno*-6,8-$C_2B_7H_{13}$ for any reaction to occur.[1b] The acidic properties of *arachno*-

(23) (a) Rudolph, R. W.; Thompson, D. A. *Inorg. Chem.* **1974**, *13*, 2779−2782. (b) Williams, R. E. *Adv. Inorg. Chem. Radiochem.* **1976**, *18*, 67−142.

(24) (a) Willie, A. E.; Su, K.; Carroll, P. J.; Sneddon, L. G. *J. Am. Chem. Soc.* **1996**, *118*, 6407−6421. (b) Grüner, B.; Jelinek, T.; Plzak, Z.; Kennedy, J. D.; Ormsby, D. L. Greatrex, R.; Stibr, B. *Angew. Chem., Int. Ed.* **1999**, *38*, 1806−1808.

6,8-$C_2B_7H_{13}$, coupled with the fact that nitriles are known to be activated by acids,[25] suggests that the 6-CH_3-*nido*-5,6,9-$C_3B_7H_9^-$ synthesis is an acid-catalyzed reaction requiring the initial protonation of the nitrile by the neutral *arachno*-6,8-$C_2B_7H_{13}$ acid in order to activate the nitrile carbon for the nucleophilic attack by the *arachno*-6,8-$C_2B_7H_{12}^-$ anion. Likewise, as described above, when $\mathbf{3}^-$ was heated in the absence of **3**, no reaction occurred, whereas in its presence, **5** was formed. Thus, a reasonable reaction sequence (Figure 10) leading to the formation of **5** can be postulated as the following: (1) protonation of the acrylonitrile by a catalytic amount of the acid **3**; (2) nucleophilic attack of the anionic carbon of $\mathbf{3}^-$ at the nitrile carbon; and (3) hydroboration and deamination of the nitrile group with concurrent insertion of the nitrile carbon into the cage at the C6 position.

The carbon insertion reaction leading to **5** is both regiospecific and stereospecific. Although **5** is obtained as an enantiomeric mixture, in each enantiomer the nitrile carbon has inserted regiospecifically at the C8−B9−B4 site in *endo*-6-R-6,8-$C_2B_7H_{11}^-$. Furthermore, as illustrated for the reactions of the two enantiomers of **3** depicted in Figure 11, since the chirality of the originally substituted cage-carbon is fixed due to the cage structure, the insertion of the nitrile carbon must occur to give the opposite chirality. Thus, if the original cage carbon has an *R*-configuration, then the inserted carbon must be of *S*-configuration, while insertion into the *S*-enantiomer will generate a new *R*-configuration cage-carbon.

(25) Schaefer, F. C. In *The Chemistry of the Cyano Group*; Rappoport, Z., Ed.; Wiley-Interscience: New York, 1970; pp 239−305.

Acknowledgment. We thank the National Science Foundation for the support of this research.

Supporting Information Available: Tables listing Cartesian coordinates and energies for DFT-optimized geometries. X-ray crystallographic data for the structure determinations of compounds $\mathbf{PSH^+2^-}$ and **3** (CIF). This material is available free of charge via the Internet at http://pubs.acs.org.

IC035357T